Nonequilibrium molecular dynamics simulations of oscillatory sliding motion in a colloidal suspension system

Hiroshi Komatsugawa and Shuichi Nosé
Department of Physics, Faculty of Science and Technology, Keio University, 3-14-1 Hiyoshi, Kohoku-ku, Yokohama, 223 Japan
(Received 14 July 1994; revised manuscript received 7 March 1995)

In the large shear region, concentrated colloidal systems exhibit two characteristic layered structures under an oscillatory shear flow [Ackerson and Pusey, Phys. Rev. Lett. **61**, 1033 (1988)]. The two structures have close packed triangular lattices stacked perpendicular to the shear rate (velocity gradient) vector but are different with the orientation of lattice vectors. The lattice is rotated by 30° or 90° at the transition point. We carried out nonequilibrium molecular dynamics simulations in a model atomic system interacting via a short range repulsive force and obtained structures corresponding well to those observed in the Ackerson-Pusey experiments. The mechanism of phase changes in this system can be explained by potential energy calculation on two sliding neighboring layers. In this model calculation, the most stable structures under oscillatory shear flows are those avoiding the overlap with particles in neighboring layers, which thereby reduce the dissipation due to shear oscillation.

PACS number(s): 62.10.+s, 64.60.−i, 62.20.−x, 82.70.−y

I. INTRODUCTION

A variety of nonequilibrium interparticle structures have been identified in colloidal suspensions undergoing a steady shear flow [1–4] and in computer simulations of atomic systems [5–8]. A typical example is the "string-order" phase discovered by Erpenbeck in molecular dynamics simulations of a hard sphere system [5]. In this phase, particles are aligned along lines parallel to the flow direction and move keeping their sequence in the line. This line is named a string. Strings are arranged in a triangular lattice in a plane perpendicular to the flow. The string-order phase has not yet been confirmed in experiments but the discovery of this structure has aroused much interest in shear induced systems.

Characteristic structural changes have been also reported in an *oscillatory* shear flow. Ackerson and Pusey carried out light scattering studies in concentrated suspensions of hard colloidal spheres [9,10]. At a volume fraction just below the freezing concentration, two successive structural changes occurred with the increase of the amplitude of the shear oscillation.

At an intermediate shear rate, their light scattering pattern corresponded to a face centered cubic (fcc) structure when the spectrum was taken in a narrow period near the extrema of the oscillation cycle. The scattering patterns at two extrema were mirror images of each other. Ackerson and Pusey interpreted their result as the sliding motion of close packed triangular lattices in the fcc structure. The close packed layers (denoted A, B, or C) are stacked normal to the velocity gradient vector. Two types of twins, $ABCABC\cdots$ and $ACBACB\cdots$ appear alternatively, synchronizing with the shear oscillation. Ackerson called this structure "fcc" order and, hereafter, we will also refer to this as a "fcc" structure.

At a higher shear rate, another structure with a hexagonal scattering pattern appeared. This was also interpreted as randomly stacked close packed layers [10]. A clear distinction between these two structures is the orientation of the basis vectors of the underlying triangular lattices. At a high shear rate, the triangular lattice is rotated by 30° or 90° around the velocity gradient vector from that in the "fcc" structure and the basis vector points in the direction parallel to the velocity vector. Ackerson called this "layer" order and we will also refer to this as a "layer" structure.

We have investigated structural changes occurring under an oscillatory shear flow by nonequilibrium molecular dynamics (NEMD) simulations [11,13–17]. In the oscillatory shear case, Morriss and Evans carried out NEMD simulations of viscoelasticity and investigated the frequency dependence of the viscosity [18]. The viscosity is obtained as a ratio of the response to artificially imposed external forces in the NEMD method. The functional form of external forces is determined so that the response of a system coincides with the requirement in the linear response theory (Green-Kubo relation) when the external forces are weak. The SLLOD algorithm is known to give the correct response even at a high shear rate, i.e., in the nonlinear region when it is employed without a thermostat [11]. When a thermostat is added to the algorithm, as we employed in our simulation, it is considered an approximation that can produce reasonable results for the transport properties [12]. We carried out simulations with particles interacting via a Weeks-Chandler-Andersen (WCA) potential because this potential reduces the computational effort. It is already known that the main features of structural changes occurring at a high shear rate do not depend much upon the choice of the potential in the steady shear case [13]. In all NEMD simulations with Lennard-Jones, hard sphere, soft sphere, or WCA potentials, qualitatively similar re-

sults have been obtained [5,7].

Preliminary simulations were carried out at several densities. However, in the present article, we report only the result at a density in the crystalline region. The transition from the "fcc" to "layer" structures occurs very clearly in this condition. A phase diagram in density–shear rate space, and further investigations on this system will be reported in a forthcoming article. The initial crystal structure changed to a new layered structure at a certain shear rate. By microscopic structure analysis, it was confirmed that this layered structure corresponds well to the "fcc" structure proposed by Ackerson and Pusey. Further increase of the shear rate induced another structural change to the "layer" structure. Thus, we obtained similar phase changes to those in colloidal suspensions in simulations with a model atomic system.

The structural changes in our system and in colloidal suspensions were analyzed on the basis of the sliding layer model. The basic assumptions of this model are the formation of close packed layered structures and the sliding of a layer relative to neighboring layers by application of the shear. We employed the sliding layer model in which a contribution of short range interactions is taken into consideration. The average potential energy over one oscillation period was used as a quantity indicating the stability of structures. By this model calculation, it is shown that both the "fcc" and "layer" structures take global minimum energy among all possible layered structures with various oscillation directions and averaged positions and the transition mechanism is explained in this model calculation.

In Sec. II, the NEMD method we employed in our simulations is reviewed [14]. We also present, in the same section, our model for the simulations of colloidal systems and how the response to the externally applied shear stress is calculated. In Sec. III, results of our simulations are presented and compared with the experimental results. The analysis of simulations based on the sliding layer model is given in Sec. IV.

II. SIMULATION METHOD AND MODEL

A. The NEMD method

Experimentally, the viscosity is defined as a ratio of the shear stress and the velocity gradient (shear rate). We consider a uniform shear deformation (Couette flow) in which the flow and the velocity gradient are parallel to the x and y axes, respectively. The viscosity η is expressed as

$$\eta = -\frac{P_{xy}}{\dot{\gamma}}, \tag{1}$$

where P_{xy} is the xy component of the stress tensor and $\dot{\gamma}$ is the shear rate,

$$\dot{\gamma} = \frac{\partial v_x}{\partial y}, \tag{2}$$

in which v_x is the x component of the velocity.

In the present article, we employed the SLLOD algorithm to calculate the response to the externally applied shear [11]. The equations of motion are

$$\dot{q_{ix}} = \frac{p_{ix}}{m_i} + \dot{\gamma} q_{iy}, \tag{3}$$

$$\dot{q_{iy}} = \frac{p_{iy}}{m_i}, \tag{4}$$

$$\dot{q_{iz}} = \frac{p_{iz}}{m_i}, \tag{5}$$

$$\dot{p_{ix}} = F_{ix} - \dot{\gamma} p_{iy} - \alpha p_{ix}, \tag{6}$$

$$\dot{p_{iy}} = F_{iy} - \alpha p_{iy}, \tag{7}$$

$$\dot{p_{iz}} = F_{iz} - \alpha p_{iz}, \tag{8}$$

where $\mathbf{q}_i$ and $\mathbf{p}_i$ are the position and the momentum of the particle i, respectively. The second terms on the right-hand side of Eq. (3) and Eq. (6) are the external fields imposed in the SLLOD algorithm.

To carry out simulations in a homogeneous condition, we also employed the Lees-Edwards periodic boundary condition [15]. The image cells in the y direction slide in the x direction with velocity; $v_{cell} = \dot{\gamma} L$, where L is the edge length of the simulation cell.

Heat is generated in this type of nonequilibrium simulations. The third terms on the right-hand side of Eqs. (6)–(8) correspond to a thermostat (the Gaussian thermostat) that removes the heat from the system and keeps the temperature at a constant value [16]. The imposition of the constraint of the constant kinetic energy is expressed as an additional term $-\alpha \mathbf{p}_i$. The expression for the undetermined multiplier α is

$$\alpha = \frac{\sum_{i=1}^{N} (\mathbf{F}_i \cdot \mathbf{p}_i - \dot{\gamma} p_{iy} p_{ix})}{\sum_{i=1}^{N} p_i^2}. \tag{9}$$

These equations of motion were integrated with a fifth-order predictor-corrector algorithm. In the thermostat in Eqs. (3)–(8), a linear streaming velocity profile is assumed. This assumption is known as the profile biased thermostat (PBT) and the inappropriateness of this type of thermostat was pointed out by Evans and Morriss [17]. In a pure particle system without solvent, the linear velocity profile cannot be maintained at a large shear rate [19]. The string phase is now considered as an artifact for an atomic system [5,20]. However, several pieces of evidence show that our model (an atomic system with a PBT) describes fairly well the behavior of colloidal suspensions [7–11,21]. In suspensions, the motion of a particle is strongly hindered by the solvent and the linear velocity profile is maintained well even at a large shear rate. Therefore, though the frictional force acting on particles from the solvent is completely ignored, the PBT seems to take it into consideration in an effective way and to describe the colloidal suspension well. The string phase is also obtained in Brownian dynamics simulations which do not employ the PBT [22,23]. We consider that our results for oscillatory shear flow also provide support for our model.

B. Model

It is known that the structures in colloidal systems are very similar to those in a hard sphere system [24,25]. The most dominant factor for structural changes is considered to be the repulsive force due to the overlap of atomic cores. Under nonequilibrium conditions, very strong driving forces are imposed to the system. The interatomic attractive forces are less important in this situation. For hard sphere, soft sphere, and Lennard-Jones systems, a similar transition from fluid to the string phase is observed in simulations under steady shear flows.

We employed an atomic system interacting via the WCA potential to simulate the colloidal suspension system,

$$\phi(r) = 4\epsilon\left\{\left(\frac{\sigma}{r}\right)^{12} - \left(\frac{\sigma}{r}\right)^{6}\right\} + \epsilon \qquad (r < 2^{\frac{1}{6}}\sigma),$$

$$\phi(r) = 0 \quad (r > 2^{\frac{1}{6}}\sigma), \tag{10}$$

which is a Lennard-Jones potential truncated at $r_c = 2^{1/6}\sigma$ and expresses the "short range" repulsive interaction between colloidal particles.

Reduced units with the characteristic energy ϵ, the length σ, and the mass of a particle m are introduced. Then, the unit of time is $(m\sigma^2/\epsilon)^{1/2}$ and the unit of temperature is ϵ/k. We start our simulations from two types of initial configurations. They are the fcc crystals whose (100) or (111) vectors point parallel to the velocity gradient vector (the y axis). The system size N for (100) orientation is 256 or 1372. In the (111) case, we employed a 504 particle system. The simulation cell consists of $3 \times 4 \times 7$ orthorhombic unit cells with edge lengths (7.776, 8.248, 7.857) containing six particles in each of them. This system size is selected so that the shape of the simulation cell becomes very close to a cube. The simulations were carried out at $T = 0.75$ and $\rho = 1.0$. Since the WCA potential has the triple point at $\rho = 0.93$ and $T = 0.75$, our initial condition corresponds to a crystalline state. We introduce the sinusoidally changing shear rate $\dot{\gamma}(t) = \gamma_0 \cos(\omega_0 t)$, where γ_0 is the amplitude of shear rate and ω_0 is the frequency. The value of ω_0 is 4.0, and unit time δt is $\pi/2000$. Then one oscillation cycle corresponds to 500 time steps. The viscosity is averaged over 80 cycles after 80 cycles of equilibration.

C. The frequency-dependent shear stress

The transport coefficient in the time-dependent case is defined as the ratio of the Fourier-Laplace transforms of P_{xy} and $\dot{\gamma}$.

$$\eta(\omega) = \frac{P_{xy}(\omega)}{\dot{\gamma}(\omega)} = \frac{P_{xy}(\omega)}{\gamma_0}\delta(\omega - \omega_0), \tag{11}$$

where $P_{xy}(\omega)$ denotes the temporal Fourier Laplace transform of the shear stress $P_{xy}(t)$ and $\delta(\omega)$ is the δ function.

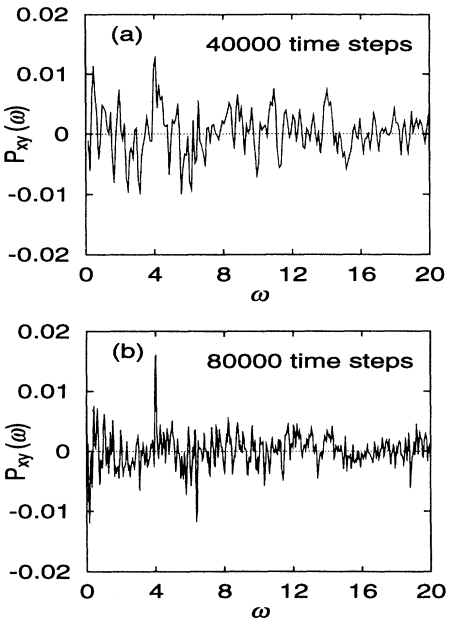

FIG. 1. Comparison of frequency spectra of $P_{xy}(\omega)$ in simulations with (a) 40 000 and (b) 80 000 time steps. The real part is shown in this figure. The frequency of applied shear ω_0 is 4.0, δt is $\pi/1000$, and the amplitude γ_0 is 0.1.

To check our algorithm, we calculated the frequency dependence of the viscosity $\eta(\omega)$ at very small shear amplitude ($\gamma_0 = 0.1$) in liquid state at $\rho = 0.6$ and $T = 1.1$ in a 256 particle system. This is the same condition as reported in Allen and Maréchal [26]. In the small shear region, the hydrodynamical effect is so weak that the systematic response of $P_{xy}(t)$ to the shear rate is hidden in large thermal fluctuations. Therefore, long simulations over many oscillation cycles are required to obtain a significant signal in the Fourier Laplace transform of $P_{xy}(t)$. To check this point, we calculated the real parts of $P_{xy}(\omega)$ for two runs, where the number of cycles in each run is

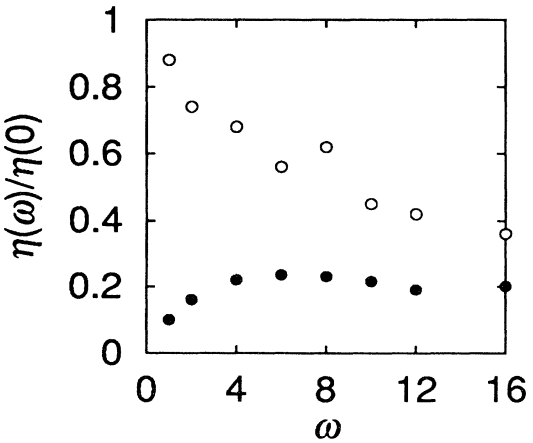

FIG. 2. The frequency dependence of $\eta(\omega_0)$ at very small strain amplitude ($\gamma_0 = 0.1$) in a liquid state at $\rho = 0.6$ and $T = 1.1$. Open and solid circles indicate real and imaginary parts of $\eta(\omega_0)$, respectively.

160 and 320. The frequency ω_0 is 4.0 and δt is $\pi/1000$ in both runs. Results are shown in Fig. 1. The signal at $\omega_0 = 4.0$ is clearly seen in 320 cycles, contrary to the obscure signal in 160 cycles. Thus, in a series of simulations in this subsection, we used 320–400 cycles to calculate the transport coefficients. The frequency dependence of $\eta(\omega_0)$ at $\gamma_0 = 0.1$ is shown in Fig. 2. The open and solid circles indicate real and imaginary parts of $\eta(\omega_0)$, respectively. These $\eta(\omega_0)$ curves are in good agreement with the result reported in Allen and Maréchal. In this way, we confirmed that our program works well even in the time-dependent case.

In the Maxwell model of viscoelasticity, the complex viscosity is expressed as

$$\eta = \frac{\eta_0}{1 - i\omega\tau}, \tag{12}$$

where η_0 is the viscosity at zero frequency and τ is the characteristic relaxation time. Our results in Fig. 2 cannot be expressed in a simple relation of Eq. (12), but the phenomenological interpretation that the response is viscous at low frequency and elastic at high frequency is also plausible [26,27]. We chose the frequency $\omega_0 = 4.0$ close to the maximum of the imaginary parts of $\eta(\omega_0)$, i.e., the inverse of the relaxation time, in the following simulations.

III. RESULTS

A. Structure changes in the (100) fcc case

The γ_0 dependence of structural and dynamical behavior in the oscillatory shear flow is studied in simulations started from an initial configuration with the fcc crystal whose (100) plane is parallel to the y-z plane. The γ_0 dependence of the real parts of $\eta(\omega_0)$ is shown in Fig. 3. At a small shear amplitude ($\gamma_0 < 0.90$), the crystal keeps its original structure but $\eta(\omega_0)$ increases rapidly with γ_0. Then at about $\gamma_0 = 0.9$, $\eta(\omega_0)$ decreases suddenly. This suggests the structure changes from the initial fcc crystal to another structure. Another structural change at $\gamma_0 = 1.8$ is also indicated in Fig. 3.

We repeated our simulations with 1372 particles to investigate the microscopic structure in more detail in each region. At first, we investigated the structure at $\gamma_0 = 1.3$ in the intermediate region. The particle configurations projected onto the y-z plane are depicted in Fig. 4 at (a) 60 000, (b) 60 250, (c) 60 500, and (d) 60 750 time steps, which correspond to 0, 1/4, 1/2, and 3/4 cycles of the shear oscillation. The shear strain vanishes at 0 and 1/2 cycles. Layered structures normal to the y axis are always visible throughout one cycle. In each layer in the x-z plane, the particles align regularly and oscillate in response to the shear. The deviation of particles from one layer and movement to another layer are not observed. In Fig. 4, layers normal to the y axis are tilted. This tilt occurs by the connection of a layer to the neighboring layer by the periodic boundary condition in the z

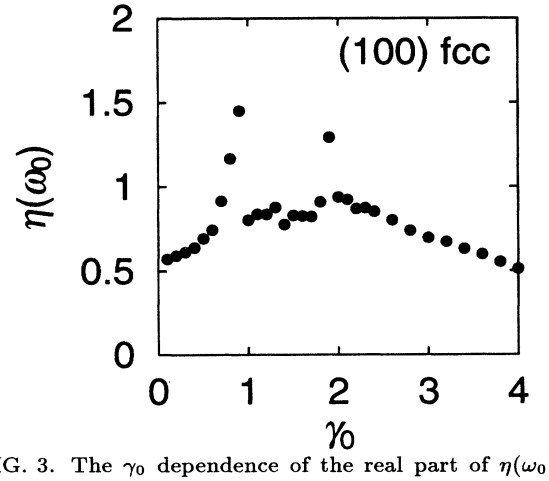

FIG. 3. The γ_0 dependence of the real part of $\eta(\omega_0)$, at $\rho = 1.0$ and $T = 0.75$. The initial configuration is the (100) fcc crystal. Two characteristic peaks at $\gamma_0 = 0.9$ and 1.8 are observed.

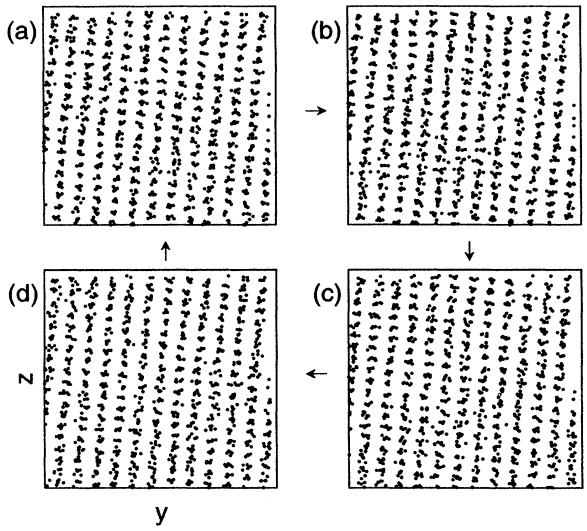

FIG. 4. Particle configurations projected onto the y-z plane in the "fcc" structure at $\gamma_0 = 1.3$. (a), (b), (c), and (d) represent 0, 1/4, 1/2, and 3/4 of oscillation cycles, respectively. The shear strain vanishes at 0 and 1/2 cycles.

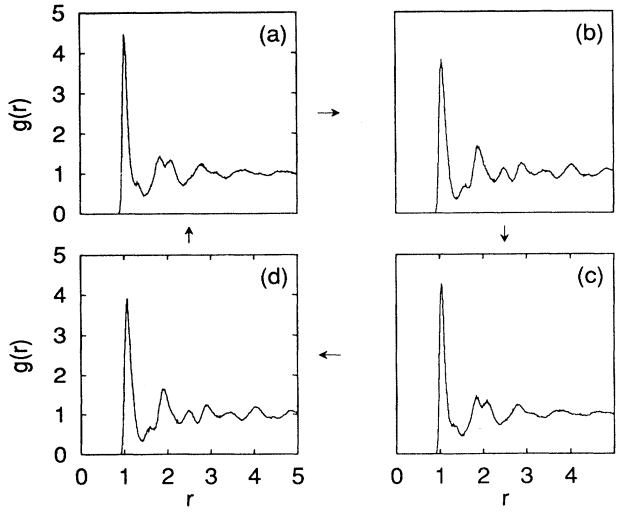

FIG. 5. Change of the pair radial distribution function $g(r)$ in the "fcc" structure at $\gamma_0 = 1.3$. The notation is the same as in Fig. 4.

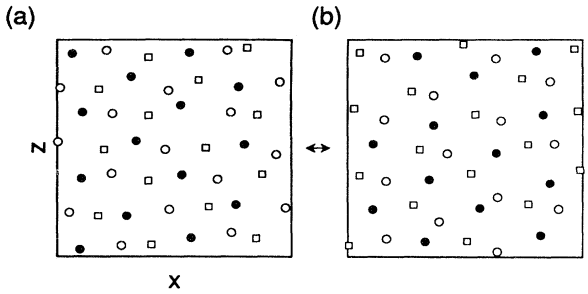

FIG. 6. Particle configurations projected onto the x-z plane in the "fcc" structure at $\gamma_0 = 1.3$. (a) and (b) represent 1/4 and 3/4 cycles corresponding to Figs. 4(b) and (d), respectively. The symbols ○, ●, and □ represent particles in the top, the middle, and the bottom layers, respectively.

direction. We repeated similar simulations many times and got tilted structures in the majority of runs. This type of mismatching, due to the periodic boundary condition, is well known in crystalline structures obtained by simulations of homogeneous nucleation. In Fig. 5, the changes of the pair radial distribution functions at the same time cycles as in Fig. 4 are shown. Each pair radial distribution function is obtained by averaging over five time cycles. At 1/4 and 3/4 cycles when the shear strain in the flow reaches extrema, the pair radial distribution functions have the peaks at $\sqrt{1}, \sqrt{2}, \sqrt{3}, \sqrt{4}, \ldots$ times of the first one. This is the pattern expected in the fcc crystal.

In the "fcc" structure proposed by Ackerson and Pusey, the sliding of the layers is synchronized with the shear oscillation between two types of fcc twins. We investigated the arrangements of particles in each layer to confirm this dynamical picture. The projections of particle positions onto the x-z plane are depicted in Fig. 6 at 1/4 and 3/4 cycles corresponding to Figs. 4(b) and (d). The symbols ○, ●, and □ represent the particles in the top, the middle, and the bottom layers, respectively. The direction of the basis vectors connecting two nearest neighbor particles is parallel to the z axis. These structures are consistent with the ABC [Fig. 6(a)] and the ACB [Fig. 6(b)] stacking. They are mirror images of each other. Therefore, our results clearly show the oscillation between twins of the fcc structure.

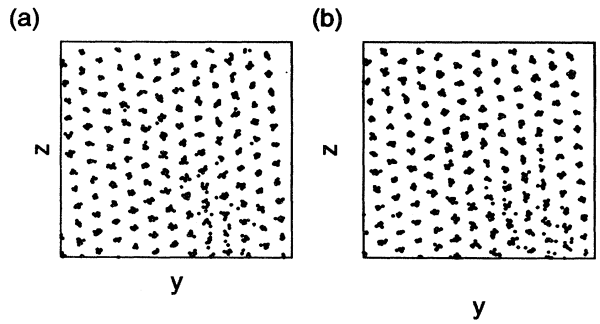

FIG. 7. Particle configurations projected onto the y-z planes of the "layer" structure at $\gamma_0 = 4.0$. (a) and (b) represent 0 and 1/4 cycles, respectively.

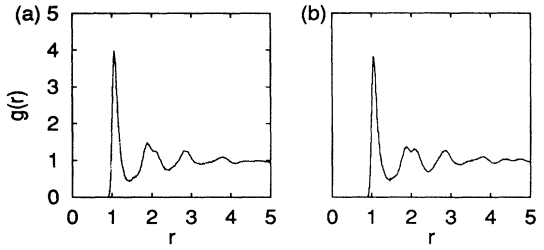

FIG. 8. Change of the pair radial distribution function $g(r)$ in the "layer" structure at $\gamma_0 = 4.0$. (a) and (b) represent 0 and 1/4 cycles, respectively. $g(r)$ does not have the second peaks seen in the "fcc" structure.

In this simulation starting from the (100) fcc crystal, the initial crystalline structure is broken at $\gamma_0 = 0.90$, and the particles reform the (111) fcc structure in which triangular lattices are stacked perpendicular to the y axis. However, the number of the particles in this simulation ($N = 4 \times 7 \times 7 \times 7$) in the initial (100) frame does not allow a perfect arrangement in the (111) fcc orientation. Therefore, the fcc structure appearing at the extrema of shear oscillation is distorted. The particle arrangement deviates considerably from perfect triangular lattices and there exist many lattice defects. Nevertheless, the structure at $\gamma_0 = 1.3$ agrees very well with the "fcc" structure concluded from the experimental results. Note that we also carried out simulations starting from an amorphous structure prepared by the quenching of the liquid state and the same structural change described here is also observed.

Next, we show the result at $\gamma_0 = 4.0$, i.e., in the region beyond the second structural change (recall Fig. 3). The projections of all particles onto the y-z plane and the pair radial distribution functions at 1/4 and 3/4 cycles are shown in Figs. 7 and 8. At both $\gamma_0 = 1.3$ and $\gamma_0 = 4.0$, the stacked layers of the close packed triangular lattices are formed parallel to x-z planes, but the orientation of the lattice is different. The projection of particle positions in one x-z layer at $\gamma_0 = 4.0$ is depicted in Fig. 9. The bond vector is parallel to the x axis at $\gamma_0 = 4.0$. The orientation of the triangular lattice is rotated by 30° or 90° from the direction at $\gamma_0 = 1.3$. At 1/4 cycle, close packed layers have a tendency to register

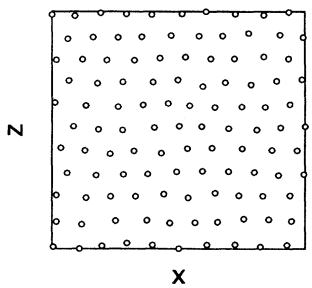

FIG. 9. Particle configuration in one layer perpendicular to the y axis in the "layer" structure at $\gamma_0 = 4.0$. The orientation of the triangular lattice is rotated by 30° or 90° from that in "fcc" structure.

so that each particle is situated over the center of a close packed triangle of atoms in neighboring layers, but the stacking of the layers is rather random in contrast with the systematic $ABCABC\cdots$ stacking in the fcc structure. The pair radial distribution function keeps almost the same shape and indicates not the "fcc" structure but a structure similar to disordered phase throughout one cycle. Therefore, this structure agrees very well with the "layer" structure observed by Ackerson and Pusey.

B. Structure changes in the (111) fcc case

In the preceding section, we reported the shear induced structural changes in the simulation starting from the (100) fcc crystal. At γ_0 larger than 0.9, the initial crystal changes into the "fcc" structure where the y axis is parallel to the (111) direction. When the shear is applied parallel to the x axis, the layers with the (111) stacking can slide more easily than those with the (100) stacking because the distance between layers is larger in the (111) stacking. The distance is $(1/2)^{1/2}a$ in the (100) fcc crystal and $(2/3)^{1/2}a$ in the (111) fcc crystal, where a is the distance between the nearest neighbor pairs. Therefore, it is reasonable to transform from the (100) fcc crystal into the "fcc" structure with the increase of γ_0.

If the (100) fcc crystal is less stable than the (111) fcc crystal under shear oscillation, the structural change from the (100) fcc crystal to the "fcc" structure might be an artifact due to an inappropriate initial condition. Therefore, we also carried out the simulation under an initial configuration of the (111) fcc crystal. In this simulation, the "fcc" structure has no lattice defects. We hoped that we could investigate the transition from the "fcc" to "layer" structures very clearly.

The γ_0 dependence of $\eta(\omega_0)$ is shown in Fig. 10. Again, $\eta(\omega_0)$ has two peaks at $\gamma_0 = 0.6$ and 2.6. From the investigation of the structures, we conclude that the second peak at $\gamma_0 = 2.6$ corresponds to the transition between the "fcc" and "layer" structures also observed in Sec. III A. Throughout this transition, the number of layers and the distance between layers do not change but the lattice is rotated by 30° or 90°.

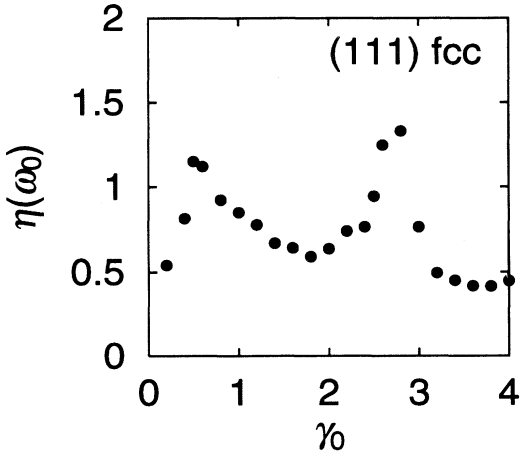

FIG. 10. The γ_0 dependence of the real part of $\eta(\omega_0)$, at $\rho = 1.0$ and $T = 0.75$. The initial configuration is the (111) fcc crystal. Two characteristic peaks at $\gamma_0 = 0.6$ and 2.6 are observed.

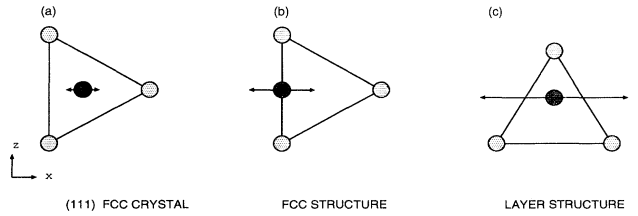

FIG. 11. Three typical structures appearing in oscillatory shear flow. (a) (111) fcc, (b) "fcc," and (c) "layer" structures. The average position and the oscillation relative to the neighboring layer are depicted.

Near the first peak, the triangular lattice in each layer is neither broken nor rotated. Why does $\eta(\omega_0)$ have a peak even though the system keeps the same lattice structure? The detailed mechanism will be presented in the next section but a qualitative explanation is as follows. When the amplitude of shear oscillation is very small, a particle oscillates around the lattice position in a static fcc crystal. The average particle position is situated just over the center of an atomic triangle in a neighboring layer. This situation is depicted in Fig. 11(a). On the other hand, oscillation between two types of fcc twins occurs in the "fcc" structure. A particle must move from the center point of a triangle to the center of the neighboring triangles. The average position is situated just over the midpoint of the edge of a triangle. This is depicted in Fig. 11(b). Therefore, the difference between these two structures near $\gamma_0 = 0.6$ is the registration of one layer relative to the neighboring layer. The average position moves from the center of the triangle to the midpoint of the edge at $\gamma_0 = 0.6$.

IV. DISCUSSION

A. The sliding layer model

In our simulations at $\rho = 1.0$, two structures, "fcc" and "layer" structures in Ackerson's notation, are observed both in the (100) fcc and the (111) fcc cases. In this section, we analyze the mechanism of a series of structural changes and the stability among structures by means of a simple model calculation based on the sliding of the rigid layers.

We consider structures in which triangular lattices are stacked parallel to the x-z plane. Each layer is rigid and does not deform during shear oscillation and only the sliding between neighboring layers is allowed in this model. This type of structures in a colloidal system undergoing the shear was proposed by Hoffman in the steady shear case [4]. Hoffman explained the appearance of an ordered structure at a high shear rate in his model. The shear viscosity becomes smaller in an ordered structure than a random one under an applied shear. Tomita and Van de Ven studied the compression of layers in the shear gradient direction in their model [28]. A similar model is introduced by Ackerson to explain the experimental results under oscillatory shear flows [10]. Ackerson studied the condition in which the hard sphere particles contact each other. The stability limit of the "fcc" structure can be explained in this way. But the relative

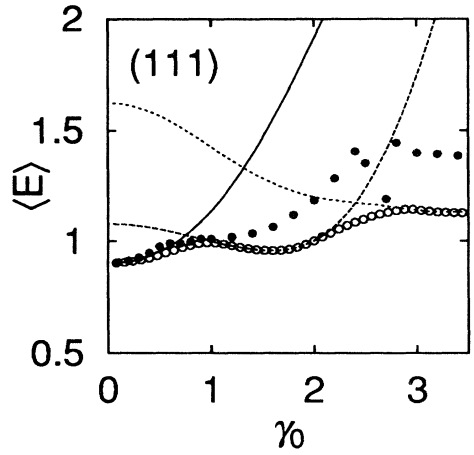

FIG. 12. γ_0 dependence of the average potential energy $\langle E \rangle$. The solid, dashed, and dotted lines and open circles indicate (111) fcc, "fcc", "layer" structures and the global minimum curve in the sliding layer model, respectively. Solid circles are the results obtained in MD simulations starting from a (111) fcc crystal.

stability between "fcc" and "layer" structures is not determined. Ackerson considered that the "layer" structure would appear after the "fcc" structure became unstable. On the other hand, our rigid energy calculation clarifies not only the stability between these two structures but also predicts the most stable state among all possible layered structures with different oscillation directions and average particle positions.

We assume the sliding of layers to be uniform in the shear gradient direction and a WCA potential between the particles. Therefore, it is sufficient to consider the relative sliding of two layers, A and B. In some cases, this simplification is not appropriate. For example, in the hcp structure where the layers stack in $ABAB\cdots$ fashion, the relative motions of A-B and B-A layers under the shear are not equivalent. A unit of three layers ABA should be taken into consideration in this case. We are interested in fcc or $ABCABC$ stacking most of time, where the relation of A-B, B-C, and A-C is equivalent. The relative motion of a particle in the layer A to the layer B is

$$x_i^A = \langle x_i^A \rangle + \frac{\gamma_0}{\omega_0} y_{AB} \sin \omega_0 t. \tag{13}$$

The parameters in this sliding are $\langle x_i^A \rangle$, the average position of the particle relative to the triangular lattice in the layer B; y_{AB}, the distance between layers, in the (111) fcc case, $y_{AB} = (2/3)^{1/2}a$; the direction of oscillation; and γ_0/ω_0, the amplitude of oscillation. The average of the potential energy is calculated over one oscillation period. We consider that the potential energy is a good quantity to estimate the stability of structures in this situation because the MD simulations were carried out at constant temperature. Moreover, there is no extra entropy arising from the lattice defects because we consider the sliding of rigid layers. Therefore, the potential energy will dominate the free energy of the system.

B. The (111) fcc case

At first, we compare the stability of the structures in simulations starting from the (111) fcc structure. Three typical structures are as follows:

(a) The (111) fcc crystal. The motion of layers occurs near the static fcc structure. The particles are situated over the center of the triangular lattice of the neighboring layer. Oscillation along the x direction indicated in Fig. 11(a) is the most stable one at small γ_0. The γ_0 dependence of this structure is given by the solid curve

TABLE I. The numerical values obtained in the MD simulation and the model calculation when γ_0 is increased in the (111) fcc case. $\langle E_{MD} \rangle$ and P are the time averaged potential energy and the pressure of one particle and $\langle E_{model} \rangle$ is the time averaged potential energy from the model calculation. η_{real} and η_{imag} are the real and imaginary parts of $\eta(\omega_0)$.

γ_0	$\langle E_{MD} \rangle$	$\langle E_{model} \rangle$	P	η_{real}	η_{imag}
0.2	0.9127	0.9098	1.912×10^{-2}	0.5976	1.8478
0.4	0.9472	0.9247	1.969×10^{-2}	0.7373	1.7438
0.6	0.9899	0.9590	2.037×10^{-2}	1.1830	0.5843
0.8	0.9990	0.9804	2.037×10^{-2}	0.9596	0.3374
1.0	1.0099	0.9599	2.065×10^{-2}	0.8140	0.3056
1.2	1.0179	0.9790	2.075×10^{-2}	0.7300	0.2838
1.4	1.0354	0.9615	2.099×10^{-2}	0.6459	0.3132
1.6	1.0642	0.9572	2.137×10^{-2}	0.6062	0.3390
1.8	1.1193	0.9722	2.211×10^{-2}	0.6049	0.3866
2.0	1.1841	1.0012	2.296×10^{-2}	0.6600	0.5138
2.2	1.2820	1.0532	2.432×10^{-2}	0.7353	0.5101
2.4	1.4039	1.0846	2.595×10^{-2}	0.7858	0.4869
2.6	2.0741	1.1212	3.475×10^{-2}	1.2821	0.2508
2.8	1.4427	1.1372	2.655×10^{-2}	0.7004	0.0846
3.0	2.7710	1.1349	2.589×10^{-2}	0.5196	0.0426
3.2	2.7628	1.1319	2.580×10^{-2}	0.4728	0.0576
3.4	2.7461	1.1282	2.564×10^{-2}	0.4402	0.0729
3.6	2.7581	1.1292	2.570×10^{-2}	0.3974	0.1255
3.8	2.7864	1.1282	2.587×10^{-2}	0.4144	0.1392
4.0	2.9186	1.1189	2.678×10^{-2}	0.4444	0.1144

in Fig. 12.

(b) The "fcc" structure. At γ_0 larger than 0.7, the (111) fcc crystal is not stable in comparison with the "fcc" structure. Oscillation at a large amplitude has a disadvantage with respect to the overlap with particles in the underlying triangular lattice. If the average position is situated over the midpoint of the edge of the triangle, the structure is unstable at small amplitude but the average of the potential energy over one cycle decreases with γ_0. In the most favorable condition, the particle visits two stable positions alternately passing over a barrier at the midpoint of the edge. This is shown in Fig. 11(b). The change of the potential energy in this structure is given by the dashed curve in Fig. 12. The potential energy reaches a minimum at $\gamma_0 = 1.6$.

(c) The "layer" structure. If the amplitude of shear oscillation is increased further in the "fcc" structure, a particle will overlap with particles in the underlying layer. Therefore, the "fcc" structure becomes unstable at larger γ_0. Sliding with the direction indicated in Fig. 11(c) is then more favorable. In this way, the overlap with particles in the underlying layer can be avoided. The potential energy of this structure is shown by the dotted curve in Fig. 12. These three curves intersect at $\gamma_0 = 0.7$ and 2.4. This suggests the successive transitions from the (111) fcc crystal to the "fcc" structure and the "layer" structure. The behavior of the potential energy corresponds well with the two peaks at $\gamma_0 = 0.6$ and $\gamma_0 = 2.6$ of $\eta(\omega_0)$ in Fig. 10. The good agreement with the simulations supports the merit of the sliding layer model.

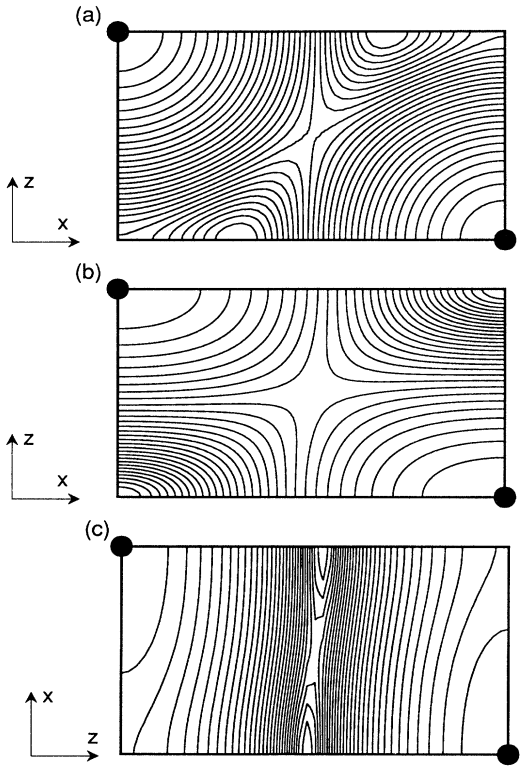

FIG. 13. The potential energy contours. (a) (111) fcc crystal at $\gamma_0 = 0.5$, (b) "fcc" structure at $\gamma_0 = 1.5$, (c) "layer" structure at $\gamma_0 = 4.0$. The energy value is large near the particles in the neighboring layer, which is indicated by circles.

We have compared the stability of three typical structures. In our model, we can also determine the most stable structure at each γ_0 value by changing the average position $\langle x_i^A \rangle$ and the oscillation direction. This potential energy curve is shown by open circles in Fig. 12. The numerical values of the time averaged potential energy from the molecular dynamics (MD) simulation and the global minimum energy of the model calculation are given in Table I. At small γ_0, the global minimum curve agrees with that of the (111) fcc structure. The potential energy contour at $\gamma_0 = 0.5$ is depicted in Fig. 13(a). The contour lines are plotted on a logarithmic scale. The averaged potential energy at each $\langle x_i^A \rangle$ is shown in this figure. The solid circles indicate the positions of particles in the neighboring layer and the potential energy becomes high near these points. At $\gamma_0 = 0.5$, the minimum is situated very close to the center of the triangular lattice. With the increase of γ_0, the energy curve of the global minimum deviates from that of the (111) fcc structure because the position of the energy minimum moves gradually to the middle of the edge. At $\gamma_0 = 1.0$, the minimum reaches the edge and remains there after that. The contour at $\gamma_0 = 1.5$ is depicted in Fig. 13(b). Here, the minimum is situated on the edge of the triangle. To confirm this structural change, we calculated the averaged particle position in the (111) fcc and "fcc" structures in the MD simulations. This is shown in Fig. 14. The midpoint of the edge of a triangle is chosen as the origin. The displacement from the origin is depicted in this figure. Contrary to the continuous change predicted in the model calculation, a discontinuous change occurs in the MD calculation.

Near the second transition point, the global minimum curve also deviates from that of the "fcc" structure. The direction of the shear oscillation deviates now from the direction in Fig. 11(b). At $\gamma_0 = 2.6$, oscillation along the direction rotated by 30° from the "fcc" case becomes most stable. The energy contour at $\gamma_0 = 3.0$ is shown in Fig. 13(c). Now, the amplitude of the oscillation is as

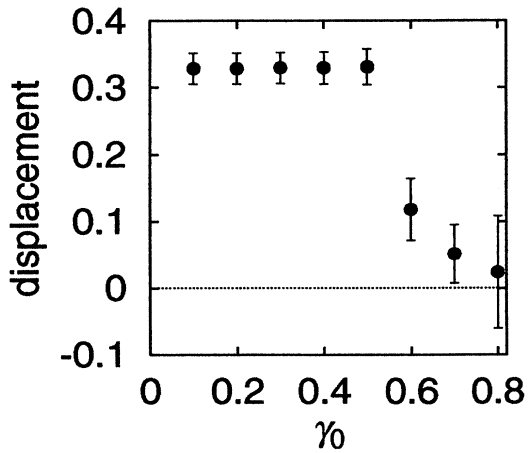

FIG. 14. The γ_0 dependence of the average position in MD calculations. The origin is chosen on the midpoint of the edge of a triangle.

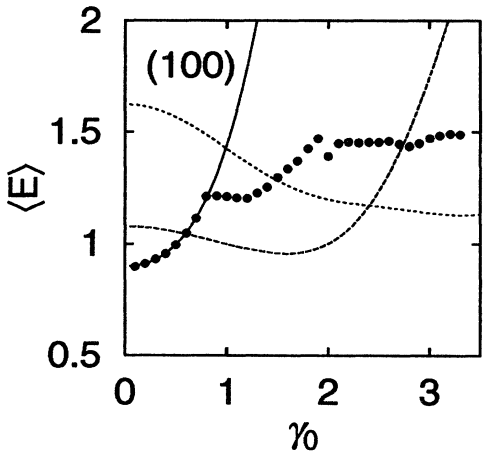

FIG. 15. The γ_0 dependence of the average potential energy. The solid line is the (100) fcc crystal and the simulation is started from a (100) fcc crystal. Other notations are the same as in Fig. 13.

large as the distance between nearest neighbor particle pairs. It is very important to avoid overlap with the particles in underlying layers. A narrow valley extends parallel to one of the bond vectors. The change of the potential energy in this valley is not large. Therefore, the required registry of neighboring layers is expected not to be so strict. This agrees very well with random stacking of layers observed in the simulations. A sudden change of the layer orientation will be observed in simulations with a periodic boundary condition because the continuous rotation of the sliding layers is prohibited.

C. The (100) fcc case

We have also applied the sliding layer model to the (100) fcc case. The sliding layers in the (100) fcc crystal are square lattices and the distance between layers y_{AB} is smaller than that in the (111) fcc structure and the overlap with particles tends to occur much more frequently. Therefore, under shear oscillation, the (100) fcc structure is expected to be less stable than the (111) fcc structure. The average potential energy over one cycle of shear oscillation is depicted in the (100) fcc case in Fig. 15. The curves of the "fcc" and "layer" structures are the same as those in the (111) fcc case. As expected, the energy of the (100) fcc crystal increases more rapidly than the (111) fcc crystal with γ_0. This confirms that the (100) fcc structure is less stable than the (111) fcc structure under the shear oscillation. The intersection between the (100) fcc and the "fcc" structures occurs at $\gamma_0 = 0.6$, which is slightly below that in the (111) fcc case. The transition point in the simulations occurs at $\gamma_0 = 0.8$ which is larger than the intersection. This type of superloading is frequently observed in the first-order phase changes. The transition from the "fcc" structure to the "layer" structure occurs at $\gamma_0 = 2.0$ in the simulations in the (100) fcc case. This transition point is smaller than the prediction in the sliding layer model and the simulations in the (111) fcc case. This disagreement will be explained as follows. In simulations starting from the (111) fcc crystal, the layer structure along the y direction is kept through the first transition at $\gamma_0 = 0.6$. Only the registry of the layers changes at this point. On the other hand, the (100) fcc structure is broken and a new layered structure is reformed. The arrangement of particles changes completely at the transition point. The number of particles in our simulations does not allow the perfect (111) type layered structure. The "fcc" structure in simulations in the (100) fcc case is distorted inevitably by lattice defects or grain boundaries and has a much higher energy than the ideal "fcc" structure in the (111) fcc case. The distorted structure is less stable and the change to the "layer" structure occurs at smaller γ_0.

V. CONCLUSIONS

In our simulations of an atomic system interacting via the WCA repulsive potential, structural changes closely corresponding with those observed in experiments on colloidal suspensions are obtained. Both of the typical structures appearing at large shear regions are layer structures in which triangular lattices are stacked perpendicular to the velocity gradient vector. The mechanism of these structural changes is explained by a simple sliding layer model. In the "fcc" structure arising at an intermediate shear, particles slide between two potential minima situated over the center of a triangle in the neighboring triangular lattices. In the "layer" structure arising at large shear, particles move along a valley parallel with the lattice vectors of triangular lattices. In these stable structures, the overlap with particles in the underlying lattice is avoided and hence dissipation is considerably reduced.

ACKNOWLEDGMENTS

The authors thank to M.L. Klein for reading the manuscript carefully. This work is supported by Grant-in-Aid for Scientific Research on Priority Areas, "Computational Physics as a New Frontier in Condensed Matter Research," from the Ministry of Education, Science, and Culture, Japan. The computations were carried out at Keio University Computer Center and at the Computer Center of the Institute for Molecular Science.

[1] B.J. Ackerson and N.A. Clark, Phys. Rev. Lett. **46**, 123 (1981).
[2] B.J. Ackerson and N.A. Clark, Phys. Rev. A **30**, 906 (1984).
[3] B.J. Ackerson, J. van der Werff, and C.G. de Kruif, Phys. Rev. A **37**, 4819 (1988).
[4] R.L. Hoffman, Trans. Soc. Rheol. **16**, 155 (1970).
[5] J.J. Erpenbeck, Phys. Rev. Lett. **9**, 1333 (1984).
[6] L.V. Woodcook, Phys. Rev. Lett. **54**, 1513 (1985).
[7] D.M. Heyes, J. Chem. Soc. Faraday Trans. 2 **82**, 1365 (1986).
[8] D.M. Heyes, J. Chem. Phys. **85**, 997 (1986).
[9] B.J. Ackerson and P.N. Pusey, Phys. Rev. Lett. **61**, 1033 (1988).
[10] B.J. Ackerson, J. Rheol. **34**, 553, (1990).
[11] D.J. Evans and G.P. Morriss, Phys. Rev. A **30**, 1528 (1984).
[12] J.W. Dufty, A. Santos, J.J. Bery, and R.F. Rodriguez, Phys. Rev. A **33**, 459 (1986).
[13] D.J. Evans and R.O. Watts, Chem. Phys. **48**, 321 (1980).
[14] D.J. Evans and G.P. Morriss, *Statistical Mechanics of Nonequilibrium Liquid* (Academic Press, New York, 1990), Chaps. 4–6.
[15] A.W. Lees and S.F. Edwards, J. Phys. C **5**, 1921 (1972).
[16] D.J. Evans, Phys. Rev. A **28**, 1016 (1983).
[17] D.J. Evans and G.P. Morriss, Phys. Rev. Lett. **52**, 1333 (1984).
[18] G.P. Morriss and D.J. Evans, Phys. Rev. A **32**, 2425 (1985).
[19] S. Hess and W. Loose, Phys. Chem. **94**, 216 (1990).
[20] D.J. Evans and G.P. Morriss, Phys. Rev. Lett. **56**, 2172 (1986).
[21] M.J. Stevens and M.O. Robbins, Phys. Rev. Lett. **66**, 3004 (1991).
[22] J.R. Melrose, Mol. Phys. **76**, 635 (1992).
[23] W. Xue and G.S. Grest, Phys. Rev. Lett. **64**, 419 (1990).
[24] M. Wadati and M. Toda, J. Phys. Soc. Jpn. **32**, 1147 (1972).
[25] S. Hachisu, Y. Kobayashi, and A. Kose, J. Colloid Interface Sci. **42**, 342 (1973).
[26] M.P. Allen and G. Maréchal, Mol. Phys. **57**, 7 (1986).
[27] D.J. Evans, Phys. Rev. A **23**, 1988 (1981).
[28] M. Tomita and T.G.M. Van de Ven, J. Colloid. Interface Sci. **99**, 374 (1984).